Spatio-temporal Phase Disambiguation in Depth Sensing

Takahiro Kushida[1], Kenichiro Tanaka[1] *Member, IEEE*, Takahito Aoto[2],
Takuya Funatomi[1], *Member, IEEE* and Yasuhiro Mukaigawa[1], *Member, IEEE*
[1]Nara Institute of Science and Technology, Ikoma, Japan
[2]University of Tsukuba, Tsukuba, Japan

Phase ambiguity is a major problem in the depth measurement in either time-of-flight or phase shifting. Resolving the ambiguity using a low frequency pattern sacrifices the depth precision, and using multiple frequencies requires a number of observations. In this paper, we propose a phase disambiguation method that combines temporal and spatial modulation so that the high depth precision is preserved while the number of observation is small. A key observation is that the phase ambiguities of temporal and spatial domains appear differently with respect to the depth. Using this difference, the phase can disambiguate for a wider range of interest. We develop a prototype to show the effectiveness of our method through real-world experiments.

Index Terms—**time-of-flight camera, phase shifting, computational photography**

I. INTRODUCTION

DEPTH measurement is widely used in applications such as 3D reconstruction, object detection, robotics, and autonomous driving. In the field of computer vision, there are two common techniques for measuring scene depth using modulated illumination. One is temporal modulation such as time-of-flight (ToF); the other is spatial modulation such as phase shifting on a pro-cam system. The temporally modulated illumination is used to measure time delays, and the spatially modulated illumination is used to find the correspondence between the projector and camera pixels for triangulation.

A common problem is how to resolve the periodic ambiguity of the phase because either measurement gives the phase that is defined between 0 to 2π. Typically, multiple frequencies are used to resolve the phase ambiguity. However, the phase ambiguity still exists in the frequency of the greatest common divisor, which requires several measurements to obtain a wider range of interest. Another possible approach is to use a low frequency that sacrifices the depth precision. The aim of this study is to resolve the phase ambiguity in fewer observations, where both the wide range of interest and the precision of the depth are guaranteed.

A key point of this paper is that the phase ambiguities of the ToF and phase shifting appear differently on the depth domain. Since the temporal phase is proportional to the depth, the depth candidates from the phase appear at equal intervals along with the depth. On the other hand, the spatial phase is defined as the disparity domain; hence, the depth candidates appear at gradually increasing intervals. Based on this difference, the phase ambiguity can be resolved by combining temporal and spatial modulation. Because the candidate that satisfies both measured phases seldom appears, the number of observations can be reduced to a single respective frequency.

In this paper, we discuss ordinary ToF and phase shifting in the same framework. We show that precise depth can be measured in a wide range by combining temporal and spatial modulation. We also reveal the conditions under which the advantage of our method is gained, and we build a prototype to show the effectiveness of our method via real-world experiments.

II. RELATED WORK

Active depth measurements have been widely studied in the computer vision field. Earlier work used a projector-camera system to convert the projector's pixel index into multiple projection images based on the gray code [1]. The phase shifting approach [2] recovers subpixel correspondences by detecting the phase of the sinusoid. Gupta *et al*. [3] unwrapped the phase from slightly different frequencies so that it became robust to indirect light transport with a small budget of projection numbers. Mirdehghan *et al*. [4] proposed an optimal code for the structured light technique.

The time-of-flight method is another way to measure depth. It emits amplitude modulated light and a delayed signal is detected that corresponds to the scene depth [5]. Because the range of interest and the depth resolution are tradeoffs, a better resolution is obtained by limiting the range of interest [6]. Another problem regarding the ToF is multi-path interference due to indirect light transport. Recovering the correct depth of multi-path scenes has been broadly studied using a parametric model [7], [8], K-sparsity [9], [10], frequency analysis [11], and data-driven approaches [12]–[14]. Because the scene depth can be recovered by the first-returning photon, the depth can be obtained after recovering light-in-flight imaging [15]–[20].

Multi-path interference is mitigated by combining ToF and projector. Naik *et al*. [21] combined the ToF camera and a projector-camera system to mitigate a multipath that uses direct-global separation [22]. Similar ideas are implemented with the ToF projectors that can modulate both spatially and temporally [23], [24]. In both cases, direct-global separation is utilized to mitigate multi-path interference.

To obtain the fine resolution, Gupta *et al*. [25] proposes the optimal code for ToF modulation. Kadambi *et al*. [26] uses the polarization cue to recover the smooth surface. An interferometer can also obtain micrometer precision. Interferometry gives micrometer precision [27] in a carefully controlled environment. Li *et al*. [28] recovered micro-resolution ToF using the superheterodyne technique. Maeda *et al*. [29] leverages the

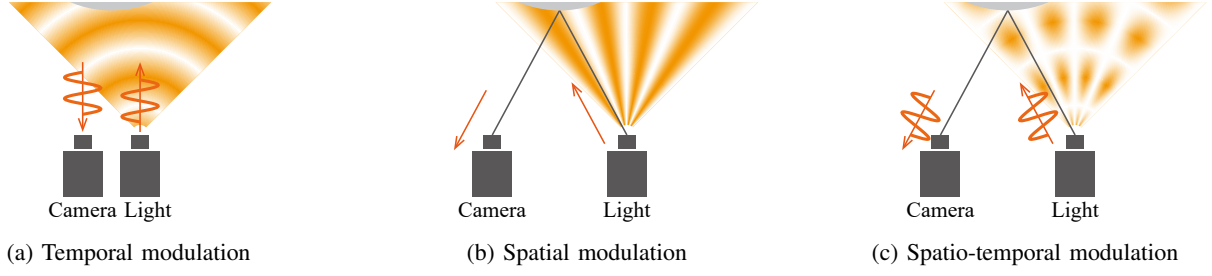(a) Temporal modulation   (b) Spatial modulation   (c) Spatio-temporal modulation

Fig. 1: Modulation variations. (a) ToF modulates the light temporally. (b) Phase shifting modulates the light spatially. (c) Our method combines temporal and spatial modulations at the same time to mitigate the phase ambiguity problem while preserving the depth precision.

heterodyne technique to the polarization imaging to obtain the accurate depth.

Phase unwrapping is a subproblem in the depth measurement. The phase has to be unwrapped with either the phase shifting or the ToF; otherwise, the estimated depth will have 2π ambiguity. The number of observations can be reduced by sacrificing the spatial resolution. The projector's coordinates can be obtained from a single image using a color code [30], a wave grid pattern [31], and a light-field ToF [32]. Our method falls into this class but does not sacrifice the spatial resolution nor require many patterns. Our method leverages the asymmetric relations of spatial and temporal wrapping to solve the ambiguity of the phase.

III. DEPTH MEASUREMENT TECHNIQUES USING MODULATED ILLUMINATION

Before explaining our method, we will briefly review the ToF and phase shifting methods. We will respectively explain them as the phase measurements using temporally or spatially modulated light.

A. Temporal modulation (time-of-flight)

The ToF camera emits the temporally modulated light as shown in Fig. 1(a). It measures the amplitude decay and phase delay of the modulated light, and the phase delay corresponds to the time it takes for the light to make a round trip.

The ToF camera measures the correlation between the signals emitted and those received. For each frequency, the phase delay is calculated from the correlations with N_T reference signals, which are temporally shifted. For the k-th signal, the correlation $c_k(x)$ at the camera pixel x is represented as

$$c_k(x) = g\left(t + \frac{2\pi k}{N_T}\right) * s(x,t) \qquad (1)$$

$$= \frac{A(x)}{2}\cos\left(\phi_T(x) + \frac{2\pi k}{N_T}\right) + O(x), \qquad (2)$$

where $g\left(t + \frac{2\pi k}{N_T}\right)$ is the reference signal with the shifted phase $2\pi k/N_T$, s is the returned signal, the $*$ operator represents the correlation, A is the amplitude decay, ϕ_T is the phase delay, and O is the ambient light. In the case of $N_T = 4$, the phase ϕ_T and the amplitude A of the returned signal can

be recovered by a direct conversion method from multiple observations while changing the phase $\frac{2\pi k}{N_T}$ as

$$\phi_T(x) = \arctan\left(\frac{c_3(x) - c_1(x)}{c_0(x) - c_2(x)}\right), \qquad (3)$$

$$A(x) = \sqrt{(c_3(x) - c_1(x))^2 + (c_0(x) - c_2(x))^2}. \qquad (4)$$

The depth d is obtained as

$$d(x) = \frac{c}{2\omega_T}\phi_T(x), \qquad (5)$$

where ω_T is the modulation frequency and c is the speed of light.

B. Spatial modulation (phase shifting)

The phase shifting spatially modulates the projection pattern. Finding the correspondences between the projector and camera pixels is the main part of the spatial phase shifting. The idea is to project the sinusoidal pattern as shown in Fig. 1(b) and measure the phase of the sinusoid for each pixel, which corresponds to the projector's pixel coordinates.

The observed intensity of the camera $I_l(x)$ for l-th shift is represented as

$$I_l(x) = A(x)\cos\left(\phi_S(x) - \frac{2\pi l}{N_S}\right) + O(x), \qquad (6)$$

where ϕ_S is the spatial phase of the projection pattern due to disparity. There are three unknown parameters, which are the offset O, the amplitude $A(x)$, and the phase $\phi_S(x)$; therefore, they can be recovered from $N_S \geq 3$ observations while changing the phase of the pattern. In the case of $N_S = 4$, the spatial phase ϕ_S and the amplitude A can be recovered in the same way as the ToF as

$$\phi_S(x) = \arctan\left(\frac{I_3(x) - I_1(x)}{I_0(x) - I_2(x)}\right), \qquad (7)$$

$$A(x) = \sqrt{(I_3(x) - I_1(x))^2 + (I_0(x) - I_2(x))^2}. \qquad (8)$$

From the estimated disparity, the scene depth can be recovered using the triangulation theory. For example, when the parallel stereo is assumed, the depth is inversely proportional to the disparity as

$$d(x) = \frac{bf}{x - \frac{\phi_S(x)}{\omega_S}} \qquad (9)$$

where $x - \frac{\phi_S}{\omega_S(x)}$ is the disparity, ω_S is the spatial angular frequency of the projection pattern, f is the focal length, and b is the baseline of the pro-cam system. Here, x represents the horizontal pixel position.

C. Phase ambiguity and depth resolution

A common problem in both temporal and spatial methods is 2π ambiguity, where the phase is wrapped when the depth exceeds the maximum depth of interest. A naïve approach is using a low frequency to avoid the phase ambiguity. However, a tradeoff exists between the range of interest and the depth precision. While the phase ambiguity does not appear at a lower frequency, the depth precision becomes low. With a higher frequency, the depth resolution improves while the phase ambiguity becomes significant, and the depth cannot be uniquely recovered for a wide range of interest.

The phase ambiguity is usually relaxed by using multiple frequencies in either a temporal or a spatial domain. We propose a hybrid approach of disambiguation that can take advantage of a different nature in temporal and spatial modulation.

IV. PROPOSED METHOD

A. Spatio-temporal modulation

We propose a hybrid method of temporal and spatial modulation as shown in Fig. 1(c). The phase ambiguity can be resolved by using both temporal and spatial phases instead of using multiple frequencies in either domain.

Our key idea is that the depth candidates from the ambiguity of the temporal and spatial phases are different. In the case of the temporal phase, the intervals of depth candidates are the same as the depth because the depth is proportional to the phase, as shown in Eq. (5). On the other hand, the spatial phase is defined in the disparity domain. Because the depth is inversely proportional to the disparity (as shown in Eq. (9)), the intervals of depth candidates increase along with the depth. Figure 2 shows the phase observations along with the scene depth. Multiple depth candidates correspond to a single phase. The depth candidates appear at the same interval for the temporal phase, while the intervals of the spatial phase increase. This difference is a key feature of our method to resolve the phase ambiguity.

Depths that satisfy both temporal and spatial phases seldom appear. The unwrapped phase is not restricted by the greatest common divisor, and the set of temporal and spatial phases is unique for the wider range of interest. The candidate depths can be respectively obtained from the following equations as

$$d_T = \frac{c}{2\omega_T}(2\pi n_T + \phi_T) \qquad (10)$$

$$d_S = \frac{bf}{x - \frac{2\pi n_S + \phi_S}{\omega_S}}. \qquad (11)$$

The integer pair (n_T, n_S) that satisfies $d_T = d_S$ seldom exists. Therefore, the phase ambiguity problem can be resolved using phases of different domains.
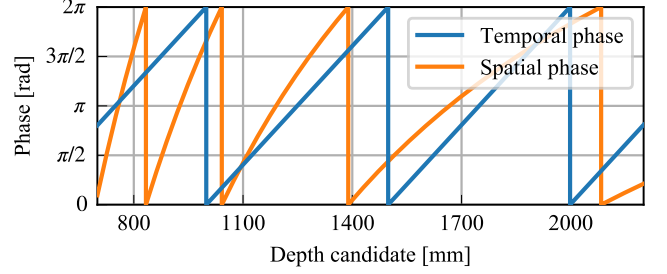

Fig. 2: Phase observations with the depth. While depth candidates of the temporal phase appear at the same intervals, those of the spatial pattern appear at increasing intervals. This difference is the cue to disambiguate the depth candidate.

B. Phase disambiguation and depth estimation

Assuming the spatial phase is fixed within the ToF accumulation period, the pixel value $c(x, k, l)$ of the k-th temporal shift and the l-th spatial shift is represented as

$$c(x, k, l) = \frac{A(x)}{2} \cos\left(\phi_S(x) - \frac{2\pi l}{N_S}\right) \cos\left(\phi_T(x) + \frac{2\pi k}{N_T}\right) + O(x). \qquad (12)$$

In the case of $N_T = 4, N_S = 2$, the temporal phase ϕ_T, and spatial phase ϕ_S are obtained as

$$\begin{cases} \phi_T(x) &= \arctan \frac{c(x,3,0)-c(x,1,0)}{c(x,0,0)-c(x,2,0)} \\ A'(x) &= \sqrt{(c(x,3,0)-c(x,1,0))^2 + (c(x,0,0)-c(x,2,0))^2} \\ O(x) &= \frac{1}{4}\sum_k \left(c(x,k,0) - A'(x)\cos(\phi_T(x) - \frac{\pi k}{2})\right) \\ \phi_S(x) &= \arctan \frac{c(x,3,1)+c(x,1,1)-2O(x)}{c(x,3,0)+c(x,1,0)-2O(x)}. \end{cases} \qquad (13)$$

Now, we have two phases: the temporal phase ϕ_T and the spatial phase ϕ_S. Depth estimation from the two phases is similar to the unwrapping problem in both the multi-frequency phase shifting and the ToF, and it can be solved by searching a lookup table [3]. The observed phases should respectively equal to the phases computed from the same depth as

$$\varphi_T(d) = \frac{2\omega_T d}{c} \bmod 2\pi \qquad (14)$$

$$\varphi_S(d, x) = \omega_S\left(x - \frac{bf}{d}\right) \bmod 2\pi. \qquad (15)$$

A lookup table is built for each horizontal pixel position x of the camera because the spatial phase depends on the pixel position. The table $\mathcal{T}_x$ at the horizontal position x consists of the vector $\Phi_{D_i,x} = [\varphi_T(D_i), \varphi_S(D_i, x)]$ of the candidate depth D_i as

$$\mathcal{T}_x(D_i) = \Phi_{D_i,x} = [\varphi_T(D_i), \varphi_S(D_i, x)]. \qquad (16)$$

For each pixel, the depth can be estimated by searching the lookup table as

$$\hat{d}(x) = \underset{d}{\arg\min} \|\mathcal{T}_x(d) - [\phi_T(x), \phi_S(x)]\|_2^2. \qquad (17)$$
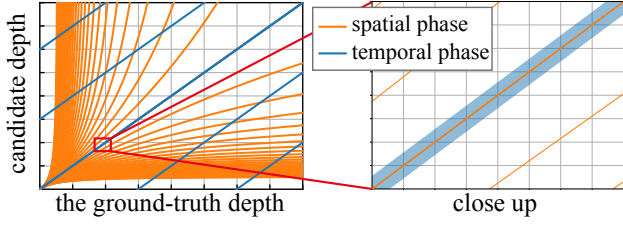
103

Fig. 3: Depth candidates of spatial and temporal phases. The blue line shows the depth candidate from the temporal phase and the orange line shows it from the spatial phase. Because the depth is inversely proportional to the spatial phase, the candidates gather at a short distance. In the close-up image, the precision of the ToF is illustrated as the width of the line. When the spatial frequency is high, the precision of the phase shifting is much better than that of the ToF.

C. Analysis of the proposed method

Frequency selection

The effectiveness of our method depends on the selection of both temporal and spatial frequencies. At least one of the frequencies should be sufficiently high to achieve better precision, because the precision will not improve if they are low. Modulating current ToF cameras at a very high frequency is difficult in practice, so we make the spatial frequency high.

Figure 3 shows the candidate depths of certain frequencies. Because the depth is inversely proportional to the spatial phase, the phase ambiguity of the spatial phase is dense at a short distance and coarse at a long distance. This property gives the bound of the spatial frequency for the designated working range. Inversely, the valid working range is determined when the spatial frequency is fixed.

1) Lower bound of the spatial frequency

When the spatial frequency is too low, the depth precision of the phase shifting becomes low, as shown in Fig. 4(a). As the depth precision of the ToF is also low, there is no benefit from combining these frequencies. The lower bound of the spatial frequency is where the depth precision of the phase shifting is better than that of the ToF, as shown in Fig. 4(b).

The precision of the spatial measurement should be better than the ToF as

$$\Delta d_S \leq \Delta d_T, \tag{18}$$

where Δd_S is the precision of the phase shifting and Δd_T is the precision of the phase shifting and the ToF, respectively. The precision is respectively represented as [5], [24]

$$\Delta d_T = \frac{c\pi}{\omega_T} \frac{\sqrt{B}}{2\sqrt{8}A}, \tag{19}$$

$$\Delta d_S = \frac{2\pi d^2}{bf\omega_S} \frac{\sqrt{B}}{2\sqrt{8}A}, \tag{20}$$

where A is the number of photo-electrons that have gathered on the sensor and represents the amplitude of the returned signal, and B is the number of photo-electrons that represents

(a) No resolution improvement

(b) Lower bound

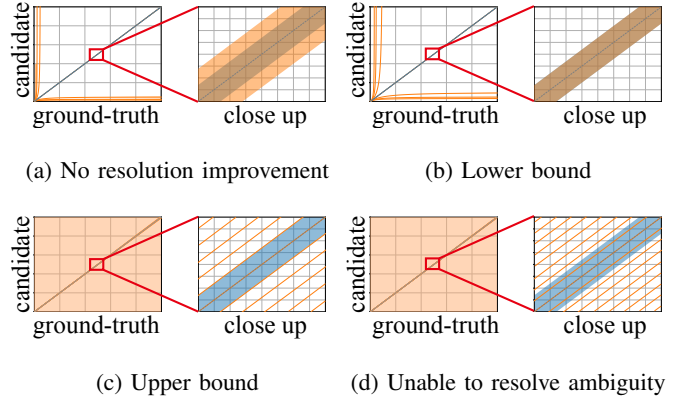(c) Upper bound

(d) Unable to resolve ambiguity

Fig. 4: Bounds to select appropriate spatial frequency. Orange lines represent the candidate depths of spatial modulation; blue lines represent the candidate depths of temporal modulation. The width of the line shows the realistic precision. Several candidates are in (c) and (d), so it looks filled. If the spatial frequency is too low (a), the precision of both frequencies is low and therefore ineffective. The precision of the spatial frequency is at least better than the ToF, as shown in (b). On the other hand, if the spatial frequency is too high, phase ambiguity cannot be resolved because multiple candidates exist within the ToF precision, as shown in (d). The upper bound of the spatial frequency is that only one line exists inside the ToF ambiguity.

the DC component of the returned signal. Finally, the lower bound of the spatial frequency is given as

$$\omega_S \geq \frac{d_{\max}^2}{bf} \frac{2\omega_T}{c}, \tag{21}$$

where $d_{\max}$ is the designated maximum working distance of the measurement system.

2) Upper bound of the spatial frequency

When the spatial frequency is too high, the phase ambiguity problem cannot be resolved because multiple candidate depths exist within the precision of the ToF, as shown in Fig. 4(d). The spatial frequency should be as high as possible unless its wrapping distance is greater than the precision of the ToF. The upper bound of the spatial frequency is where the phase wrapping distance is larger than the precision of the ToF as shown in Fig. 4(c) as

$$\frac{bf}{x - \frac{\phi_S}{\omega_S}} - \frac{bf}{x - \frac{\phi_S - 2\pi}{\omega_S}} \geq \frac{\Delta d_T}{2}. \tag{22}$$

Substituting Eq. (15) and transforming the expression, the upper bound can be obtained as

$$\omega_S \leq \frac{2\pi \left(2d_{\min}^2 + \Delta d_T d_{\min}\right)}{bf\Delta d_T}, \tag{23}$$

where $d_{\min}$ is the shortest depth of the designated working distance of the system.

The number of observations

Another benefit to combining temporal and spatial modulation is that the temporal and spatial phases can be measured at the same time without affecting each other because the time and space are orthogonal and they can be superposed.

Our method requires six correlation values to estimate two phases. These observations can be acquired by three subframes because the complementary frames of the temporal modulation can be simultaneously obtained using a typical 2-tap ToF sensor. Concretely, a set of $c(x, 0, l)$ and $c(x, 2, l)$ is simultaneously obtained, and the set of $c(x, 1, l)$ and $c(x, 3, l)$ is also obtained at a single subframe, which is the benefit of superposing spatio-temporal projection.

To reduce the number of projections, binding two pixels or sub-pixels can viably obtain the spatial phase in a single frame, which is an idea similar with a Bayer pattern. When we assume the depth and reflectance of the neighboring pixels are same, the phase of the spatial pattern is spatially shifted by $1/\omega_S$ at the neighboring pixel. In this case, the number of the subframes is reduced to 2, while we can obtain two different phases at the same time and the number of subframes is the same as an ordinary ToF.

Brightness of the pattern

One may think that the temporal phase cannot be obtained if the spatial pattern is completely black. Because the spatial sinusoidal pattern is projected, all the pixels have a chance to obtain the photons unless the spatial pattern is extremely low. Another possible solution is to add the offset to the spatial pattern so that the temporal phase can be obtained for all the pixels. Adding the constant value can affect the spatial phase estimation, so $N_S \geq 3$ is required to cancel this offset. The equation for the spatial estimation becomes the same as Eq. (7).

V. EXPERIMENT

We demonstrated the effectiveness of our method with real-world experiments.

A. Hardware prototype

We developed a hardware prototype that can illuminate a scene with a spatio-temporal modulated pattern. Our prototype was built onto a ToF camera (Texas Instruments OPT8241-CDK-EVM). The light source was replaced with a laser diode and a DMD system that can project the spatial pattern. The light source was an 830nm laser diode (Hamamatsu Photonics L9277-42), and its emission was synchronized with the ToF sensor. The light emitted by the diode was collimated and expanded through lenses, and then reflected onto a DMD device (Texas Instruments DLP6500) that had 1920×1080 pixels. Finally, the spatio-temporal pattern was projected onto the scene through a projection lens, as shown in Fig. 5.

First, the measurement system was calibrated in a standard way for the pro-cam systems using a reference board [33]. The phase of the ToF on each pixel was then calibrated to share the same coordinates as the pro-cam system. A white plane board was captured while its position was moved for the phase calibration. For each measurement of the board, the
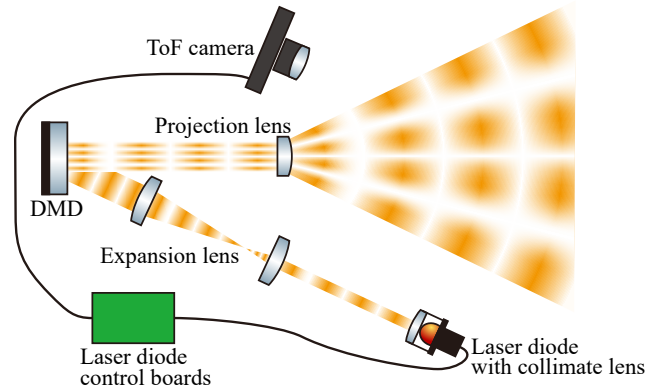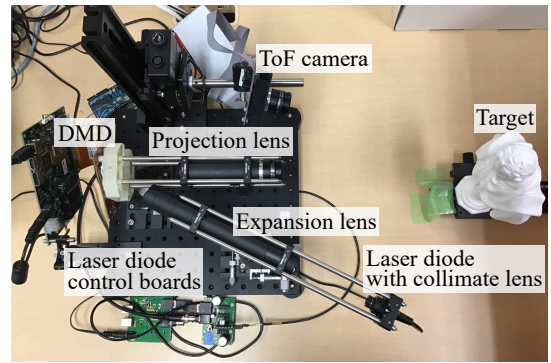

Fig. 5: Hardware prototype. The light source unit consists of a laser diode and a DMD device. The emission of the laser diode is temporally modulated by the sync signal from the ToF camera and then spatially modulated by the DMD. The ToF camera and the projection lens of the projector are placed side by side.

pair of the raw phase and the ground-truth depth was obtained because the depth of the board was measured by the ordinary phase shifting. The parameter to recover the depth from the phase was calibrated by line fitting.
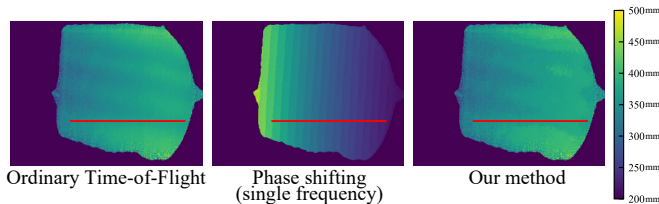
B. Result

First, we measured a white planar board and placed it at approximately 350mm from the camera and slightly slanted it, as shown in Fig. 6(a). The temporal frequency was 60MHz, and the period of the spatial pattern was 60 pixels on the projection image. The baseline between the camera and the projector was approximately 70mm, and the focal length of the projection lens was 35mm.

The depths were obtained by an ordinary ToF with a single low frequency, phase shifting with single high frequency, and our method for the comparison. Because the unique depth could not be obtained by using the phase shifting with a single high frequency due to the phase ambiguity, we added an arbitrary offset ($2\pi n_S$) to fit the global scale, but the phase wrapping is not compensated. Figure 6(b) shows the estimated depth images. Both the ToF and our method recovered the global depth while the phase shifting suffered from the ambiguity, causing the stepping pattern to appear. The cross-section of the red line is shown in Fig. 6(c). While the depth measured by the ordinary ToF is noisy and

(a) Setup

Ordinary Time-of-Flight   Phase shifting (single frequency)   Our method
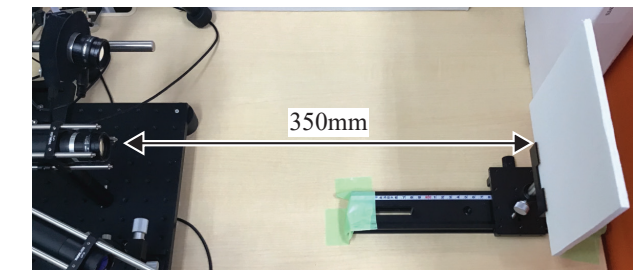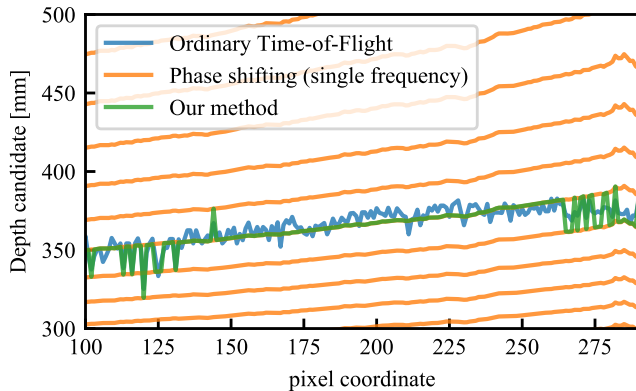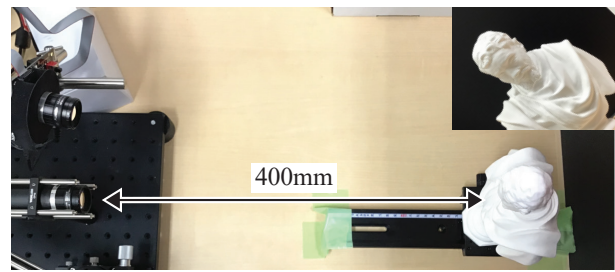
(b) Depth images

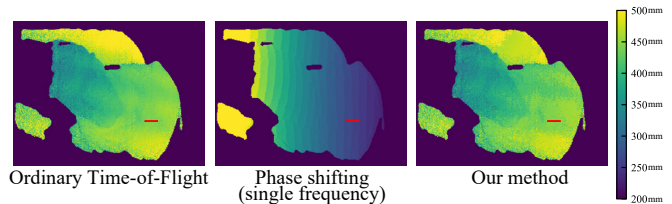(c) Cross-section of the depth image

Fig. 6: Results with a white planar board. Ordinary ToF, phase shifting (single high frequency), and our method are compared. (a) The object was placed at a slight slant. (b) The estimated depth images. Because the depth cannot be identified in the phase shifting, the wrapping ambiguity appeared as the stepping effect. (c) The cross-section of the red line is shown. While the ordinary ToF is noisy and phase shifting has many candidates, our method recovered a smooth and unique depth candidate.

there are many depth candidates due to phase ambiguity in the phase shifting, our method recovered a smooth surface while resolving the phase ambiguity. The region near the edge was not correctly disambiguated because the precision of the temporal measurement exceeded the interval of the phase shifting because the ToF precision was larger than what we expected. However, decreasing the spatial frequency might have mitigated it.
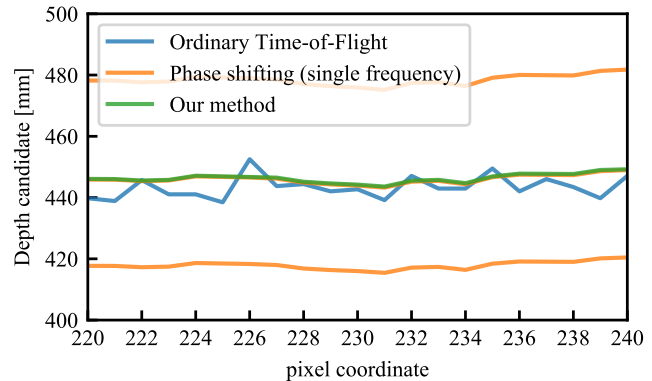
Finally, we measured a plaster bust and placed it approximately 400mm from the camera, as shown in Fig. 7(a). The estimated depth images are shown in Fig. 7(b). The cross-section of the depth is shown in Fig. 7(c). Our method recovered a unique and smooth depth.

(a) Setup

Ordinary Time-of-Flight   Phase shifting (single frequency)   Our method

(b) Depth images

(c) Cross-section of the depth image

Fig. 7: Results with a plaster bust. (a) The scene. (b) The depth maps. (c) The cross-section of the red lines drawn on (b). Our method recovered a unique and smooth surface.

VI. DISCUSSIONS

We developed a depth sensing method that uses spatio-temporally modulated illumination. We showed that the phase ambiguities of the temporal and spatial modulations are different, so it is possible to effectively resolve the ambiguities while reducing the observations and preserving the depth precision.

While our method is of interest from the viewpoint of phase wrapping, another factor contributes to the wide range of interest. Our method might not work well at a short distance because the spatial ambiguity could become smaller than the ToF precision. Using a lower frequency or narrower baseline is an option that will make a short working distance while the precision of the far region worsens. The co-design of spatial frequency, baseline, and working distance are necessary to achieve the best performance.

Our hardware prototype has some limitations. Because the DMD produces the sinusoidal pattern by controlling the mirrors on and off, it can make artifacts to the ToF. We ignored this effect, but it should be considered to control the DMD or to use a solid spatial light modulator appropriately. We also

ignored the temporal mismatch of the ToF due to the baseline. The depth measured by the ToF camera corresponds to the light path length from the light source to the camera; it is affected by a long baseline and should be compensated. In practice, the baseline is much smaller than the object depth, so it can be safely ignored.

The quality of the spatio-temporally modulated illumination of our prototype is not very high. The temporal phase contains a systematic distortion and the spatial resolution of the projector is currently limited to 64 pixels on the DMD, corresponding to 4 pixels on the camera, because the pattern is blurred. This might be due to the collimation and the alignment accuracy of the optics or the diffraction on the DMD. The light source cannot emit a spatial pattern that is equal to or less than the camera pixel's size, resulting in diminished phase shifting. In future implementations, we will develop a better light source unit to improve the temporal phase measurements and generate higher spatial resolutions.

REFERENCES

[1] S. Inokuchi, K. Sato, and F. Matsuda, "Range Imaging System for 3-d Object Recognition," in *Proc. International Conference on Pattern Recognition*, 1984, pp. 806–808.

[2] J. Salvi, S. Fernandez, T. Pribanic, and X. Llado, "A state of the art in structured light patterns for surface profilometry," *Pattern Recognition*, vol. 43, 2010.

[3] M. Gupta and S. Nayer, "Micro Phase Shifting," in *Proc. CVPR*, 2012, pp. 813–820.

[4] P. Mirdehghan, W. Chen, and K. N. Kutulakos, "Optimal structured light à la carte," in *Proc. CVPR*, June 2018.

[5] R. Lange and P. Seitz, "Solid-state time-of-flight range camera," *IEEE Journal of Quantum Electronics*, vol. 37, no. 3, pp. 390–397, mar 2001.

[6] K. Yasutomi, T. Usui, S.-m. Han, T. Takasawa, K. Keiichiro, and S. Kawahito, "A Submillimeter Range Resolution Time-of-Flight," *IEEE Transactions on Electron Devices*, vol. 63, no. 1, pp. 182–188, 2016.

[7] F. Heide, L. Xiao, A. Kolb, M. B. Hullin, and W. Heidrich, "Imaging in Scattering Media using Correlation Image Sensors and Sparse Convolutional Coding." *Optics express*, vol. 22, no. 21, pp. 26 338–50, 2014.

[8] A. Kirmani, A. Benedetti, and P. A. Chou, "Spumic: Simultaneous Phase Unwrapping and Multipath Interference Cancellation in Time-of-Flight Cameras using Spectral Methods," in *IEEE International Conference on Multimedia and Expo (ICME)*. IEEE, 2013, pp. 1–6.

[9] D. Freedman, E. Krupka, Y. Smolin, I. Leichter, and M. Schmidt, "Sra: Fast Removal of General Multipath for ToF Sensors," in *Proc. ECCV*, 2014, pp. 1–15.

[10] H. Qiao, J. Lin, Y. Liu, M. B. Hullin, and Q. Dai, "Resolving Transient Time Profile in ToF Imaging Via Log-Sum Sparse Regularization." *Optics letters*, vol. 40, no. 6, pp. 918–21, 2015.

[11] A. Kadambi, J. Schiel, and R. Raskar, "Macroscopic Interferometry: Rethinking Depth Estimation with Frequency-Domain Time-Of-Flight," in *Proc. CVPR*, 2016, pp. 893–902.

[12] J. Marco, Q. Hernandez, A. Muñoz, Y. Dong, A. Jarabo, M. H. Kim, X. Tong, and D. Gutierrez, "Deeptof: Off-the-shelf real-time correction of multipath interference in time-of-flight imaging," *ACM Trans. Graph.*, vol. 36, no. 6, pp. 219:1–219:12, Nov. 2017. [Online]. Available: http://doi.acm.org/10.1145/3130800.3130884

[13] K. Tanaka, Y. Mukaigawa, T. Funatomi, H. Kubo, Y. Matsushita, and Y. Yagi, "Material Classification from Time-of-Flight Distortions," *IEEE TPAMI*, 2018.

[14] S. Su, F. Heide, G. Wetzstein, and W. Heidrich, "Deep end-to-end time-of-flight imaging," in *Proc. CVPR*, June 2018.

[15] A. Velten, T. Willwacher, O. Gupta, A. Veeraraghavan, M. G. Bawendi, and R. Raskar, "Recovering Three-Dimensional Shape Around a Corner using Ultrafast Time-of-Flight Imaging," *Nature communications*, vol. 3, no. 745, 2012.

[16] F. Heide, M. B. Hullin, J. Gregson, and W. Heidrich, "Low-Budget Transient Imaging using Photonic Mixer Devices," *ACM ToG*, vol. 32, no. 4, p. 1, 2013.

[17] K. Kitano, T. Okamoto, K. Tanaka, T. Aoto, H. Kubo, T. Funatomi, and Y. Mukaigawa, "Recovering Temporal PSF using ToF Camera with Delayed Light Emission," *IPSJ Transaction on Computer Vision and Applications*, vol. 9, no. 15, June 2017.

[18] A. Kadambi, R. Whyte, A. Bhandari, L. Streeter, C. Barsi, A. Dorrington, and R. Raskar, "Coded Time of Flight Cameras: Sparse Deconvolution to Address Multipath Interference and Recover Time Profiles," *ACM ToG*, vol. 32, no. 6, pp. 1–10, 2013.

[19] M. O'Toole, F. Heide, L. Xiao, M. B. Hullin, W. Heidrich, and K. N. Kutulakos, "Temporal Frequency Probing for 5D Transient Analysis of Global Light Transport," *ACM ToG*, vol. 33, no. 4, pp. 1–11, 2014.

[20] M. O'Toole, F. Heide, D. Lindell, K. Zang, S. Diamond, and G. Wetzstein, "Reconstructing Transient Images from Single-Photon Sensors," in *Proc. CVPR*, 2017.

[21] N. Naik, A. Kadambi, C. Rhemann, S. Izadi, R. Raskar, and S. Bing Kang, "A Light Transport Model for Mitigating Multipath Interference in Time-of-Flight Sensors," in *Proc. CVPR*, 2015, pp. 73–81.

[22] S. K. Nayar, G. Krishnan, M. D. Grossberg, and R. Raskar, "Fast Separation of Direct and Global Components of a Scene using High Frequency Illumination," *ACM ToG*, vol. 25, no. 3, pp. 935–944, 2006.

[23] R. Whyte, L. Streeter, M. J. Cree, and A. A. Dorrington, "Resolving multiple propagation paths in time of flight range cameras using direct and global separation methods," *Optical Engineering*, vol. 54, pp. 54 – 54 – 9, 2015. [Online]. Available: https://doi.org/10.1117/1.OE.54.11.113109

[24] G. Agresti and P. Zanuttigh, "Combination of Spatially-Modulated ToF and Structured Light for MPI-Free Depth Estimation," in *ECCV Workshop on 3D Reconstruction in the Wild*, 2018.

[25] M. Gupta, A. Velten, S. K. Nayar, and E. Breitbach, "What are optimal coding functions for time-of-flight imaging?" *ACM ToG*, vol. 37, no. 2, pp. 13:1–13:18, Feb. 2018. [Online]. Available: http://doi.acm.org/10.1145/3152155

[26] A. Kadambi, V. Taamazyan, B. Shi, and R. Raskar, "Polarized 3D: High-Quality Depth Sensing with Polarization Cues," in *Proc. ICCV*, 2015, pp. 3370–3378.

[27] I. Gkioulekas, A. Levin, F. Durand, and T. Zickler, "Micron-Scale Light Transport Decomposition using Interferometry," *ACM ToG*, vol. 34, no. 4, pp. 37:1–37:14, 2015.

[28] F. Li, F. Willomitzer, P. Rangarajan, M. Gupta, A. Velten, and O. Cossairt, "Sh-tof: Micro resolution time-of-flight imaging with superheterodyne interferometry," in *Proc. ICCP*, 2018.

[29] T. Maeda, A. Kadambi, Y. Y. Schechner, and R. Raskar, "Dynamic heterodyne interferometry," in *Proc. ICCP*, 2018.

[30] R. Sagawa, H. Kawasaki, R. Furukawa, and S. Kiyota, "Dense one-shot 3d reconstruction by detecting continuous regions with parallel line projection," in *Proc. ICCV*, 2011.

[31] R. Sagawa, K. Sakashita, N. Kasuya, H. Kawasaki, R. Furukawa, and Y. Yagi, "Grid-based active stereo with single-colored wave pattern for dense one-shot 3d scan," in *3DIMPVT*, Oct 2012, pp. 363–370.

[32] S. Jayasuriya, A. Pediredla, S. Sivaramakrishnan, A. Molnar, and A. Veeraraghavan, "Depth fields: Extending light field techniques to time-of-flight imaging," in *2015 International Conference on 3D Vision*, Oct 2015, pp. 1–9.

[33] Z. Zhang, "A flexible new technique for camera calibration," *TPAMI*, vol. 22, pp. 1330 – 1334, 12 2000.